

Journal of Materials Chemistry A

Accepted Manuscript



This is an *Accepted Manuscript*, which has been through the Royal Society of Chemistry peer review process and has been accepted for publication.

Accepted Manuscripts are published online shortly after acceptance, before technical editing, formatting and proof reading. Using this free service, authors can make their results available to the community, in citable form, before we publish the edited article. We will replace this *Accepted Manuscript* with the edited and formatted *Advance Article* as soon as it is available.

You can find more information about *Accepted Manuscripts* in the [Information for Authors](#).

Please note that technical editing may introduce minor changes to the text and/or graphics, which may alter content. The journal's standard [Terms & Conditions](#) and the [Ethical guidelines](#) still apply. In no event shall the Royal Society of Chemistry be held responsible for any errors or omissions in this *Accepted Manuscript* or any consequences arising from the use of any information it contains.

ARTICLE

Supercapacitor with High Capacitance Based on Reduced Graphene Oxide/Carbon Nanotubes/NiO Composite Electrode

Cite this: DOI: 10.1039/x0xx00000x

Yang Bai, Meng Du, Jie Chang, Jing Sun*, and Lian Gao

Received 00th January 2013,
Accepted 00th January 2013

DOI: 10.1039/x0xx00000x

www.rsc.org/

We present a facile method to fabricate well-crystalline reduced graphene oxide (RGO)/carbon nanotubes (CNTs)/NiO composite for supercapacitor electrodes. The RGO/CNTs/NiO (GCN) composite takes dual advantages of CNTs and RGO. CNTs present the aggregation of RGO/NiO and improve the electron transport of GCN composite owing to its good conductivity. The restricting effect of RGO makes NiO nanoparticles have more active sites. Attributed to the uniform structure and improved electrical conductivity, GCN composite exhibits highly enhanced electrochemical performance compared with those of RGO/NiO and CNTs/NiO composites. The specific capacitance of GCN composite is about 1180 F g⁻¹ at 1 A g⁻¹ together with capacitance retention of 95 % (1000 F g⁻¹) over 2000 cycles at 4 A g⁻¹. GCN composite has been proved to be very promising as energy storage electrode materials.

1. Introduction

Electrochemical capacitors (ECs) are novel energy storage devices with high power performance, long cycle life, and low maintenance cost.¹⁻³ Usually, ECs show higher power density and longer cycle life but lower energy density than batteries. They are appropriate for devices which require short-term power or act as peak power assistances for batteries.^{3, 4} According to different energy storage mechanisms of electrode materials,⁵⁻⁷ ECs could be classified into two types, electric double layer capacitors (EDLCs) and pseudo-capacitors (PCs). EDLCs store energy via ion adsorption process and PCs via fast surface redox reactions.⁸⁻¹⁰ Carbon materials, such as active carbon (AC), carbon nanotubes (CNTs), and graphene, have large specific surface area, excellent electrical conductivity and high power density for EDLCs.¹¹⁻¹³ However, their energy densities are limited by the adsorption capacity for electrolyte ions. On the other hand, pseudo-capacitive materials include transition metal oxide/hydroxide¹⁴⁻¹⁷ and conducting polymer.¹⁸ They can provide multiple redox reactions to obtain higher capacitance. Unfortunately, low electric conductivities of these materials limit electron transport,² leading to low power densities. A major challenge in this field is to improve energy densities of ECs and simultaneously keep their high power densities.

NiO, a typical pseudo-capacitive material with high theoretical capacity, is easy to synthesize with low cost.¹⁴ It has attracted a great deal of attention to be applied in PCs. Zhang et al. synthesized porous NiO nanocolumns with relative high specific capacitance (390 F g⁻¹) than those of other morphologies.¹⁹ Cao et al. fabricated flowerlike NiO hollow nanospheres, showing high specific capacitance of 585 F g⁻¹.²⁰ Although NiO has shown relatively high capacitance, its electron and ion transport abilities are low. Apart from designing the morphology of NiO, many efforts²¹⁻²³ have been

focused on combining NiO and carbon materials to improve the conductivity.

Graphene is one of the most promising carbon materials due to its excellent electrical and mechanical properties. Among various preparation methods, chemical reduction of graphene oxide (GO) is considered as the most convenient method for bulk production.²⁴⁻²⁶ The high surface area and electrical conductivity enable the chemical derived reduced graphene oxide (RGO) to modify electrochemical materials. Zhu et al. prepared RGO/NiO electrode with high specific capacitance of 770 F g⁻¹ and enhanced rate capability.²⁷ Zhao et al. studied electrochemical properties of monolayer graphene/NiO nanosheets, which showed high specific capacitance of 525 F g⁻¹.²⁸ Electrochemical performance of these RGO based composites is significantly enhanced compared with those of pure NiO. However, the residual oxygen-containing functional groups in RGO, poor crystallinity and nonuniform structure would reduce the stability of these RGO based electrodes. Besides, RGO/NiO composites will restack easily due to intensive π - π interaction during the reaction process,²⁹ which will also shorten the cycle life of the electrodes. These issues urgently need to be solved.

Carbon nanotubes (CNTs) are another widely used carbon material to improve the conductivity of transition metal oxide.^{3, 30, 31} Ni-Co oxides/CNTs composites synthesized by Fan et al. showed a high specific capacitance of 569 F g⁻¹, as well as a good cycle life.³² Liu et al. fabricated CNTs/NiO/Ni nanocomposites with a high specific capacitance and excellent capacitive behavior.²⁸ All these results certified that CNTs were appropriate for improving the electron transport of composite electrodes. However, their poor solubility and tendency towards aggregation are not beneficial for metal oxides anchoring. Consequently, the interfacial bonding between CNTs and metal oxides is weak, leading to inferior stability of the electrodes. As far as we know, Graphene oxide can improve the dispersion of

CNTs, which preserves the electronic structure of CNTs and forms a better conductive network.²⁹

Inspired by this phenomenon, we synthesized RGO/CNTs/NiO (GCN) composite via a simple method under mild conditions. In the synthesis process, urea was used to control the hydrolysis of metal salts and reduce GO to RGO. The reagents used in this process were environmental friendly. The aggregation of RGO/NiO was successfully avoided by the addition of CNTs. The sizes of NiO particles were decreased and the conductivity of GCN composite was enhanced because of the synergistic effect of RGO and CNTs. As a consequence, GCN showed high specific capacitance of 1180 F g⁻¹ at 1 A g⁻¹. The capacitance at 4 A g⁻¹ was still as high as 1000 F g⁻¹ with the loss rate of 5 % after 2000 cycles, certifying excellent cycling stability. GCN composite has been proved to be very promising as energy storage electrode materials.

2. Experimental section

2.1 Materials preparation

Graphite was purchased from Alfa Aesar (325 mesh). Carbon nanotubes were purchased from Shanghai Chenrong electric furnace Co., Ltd. All of the other chemical reagents used in our experiments are of analytical grade, purchased from Shanghai Sinopharm Chemical Reagent Co., Ltd. (Shanghai, China). Graphene oxide (GO) was prepared from graphite flakes by modified Hummers method.³³ The as-prepared GO was dispersed in distilled water by ultrasonication, forming a yellow-brown suspension with a concentration of 1 mg mL⁻¹. Carbon nanotubes (CNTs) used in this work were pretreated with nitric acid (analytical grade). The as-received CNTs were firstly refluxed with 60% (w) HNO₃ solution at 80 °C for 6 h, then washed with distilled water and dried.

2.2 Synthesis of RGO/CNTs/NiO composite

In a typical process, 0.02 g as-received CNTs was added into 80 mL GO suspension with a concentration of 1 mg mL⁻¹ under vigorous stirring. Then, 50 mL aqueous solution containing 0.4362 g Ni(NO₃)₂·6H₂O and 1.5 g urea was slowly dropped into the GO and CNTs suspension. After stirring for 30 min, the mixture was refluxed at 100 °C for 12 h in an oil bath. The reaction product was filtrated and washed with distilled water and ethanol successively for several times. Finally, it was dried at 60 °C overnight, and then heat treated at 250 °C for 2 h in air. The obtained RGO/CNTs/NiO composite powder was denoted as GCN. With the other conditions being the same, 100 mg CNTs or GO were used as carbon source to replace GO/CNTs. The reaction products were denoted as CNO and GNO, respectively.

2.3 Characterization

Powder X-ray diffraction (XRD, Rigaku D/Max 2200PC, Cu K α) was used to characterize the crystalline structure. Raman spectroscopy was recorded on DXR Raman Microscope with an excitation length of 532 nm. X-ray photoelectron spectroscopy (XPS) analysis was conducted using twin anode gun, Mg K α (1253.6 eV) (Microlab 310F Scanning Auger Microprobe, VG SCIENTIFIC Ltd). The morphology and structure of the products were carried on field-emission scanning electron microscope (FE-SEM, Magellan 400) and transmission electron microscope (TEM, JEOL JEM-2100F).

The electrochemical properties of the materials were characterized by three-electrode system in 2 M KOH aqueous solution at room temperature. The working electrode was prepared as follows. 4 mg of CNO, GNO or GCN active materials, 0.5 mg of carbon black and 0.5 mg of polyvinylidene fluoride (PVDF) binder were mixed in ethanol, and then pasted onto a nickel foam current collector. Each working electrode was the same weight of 5 mg. Platinum wire was used as the counter electrode and Hg/HgO as the reference electrode. The electrochemical impedance spectrum (EIS) was tested by applying an AC voltage with 5 mV amplitude in a frequency range from 0.01 Hz to 100 kHz on CHI660D Workstation (Shanghai, China). The cyclic voltammetry (CV) at -0.1 - 0.65V were measured on CHI660D Workstation. The galvanostatic charge and discharge tests were carried out in the potential range of 0.1 - 0.6V on LAND CT2001 battery tester. The specific capacitances C_s were calculated from the galvanostatic discharge curves using the equation:^{5, 34}

$$C_s = \frac{it}{(\Delta v)m} \quad (1)$$

where *i*, *t*, Δv , and *m* are the constant current (A), discharge time (s), potential drop during discharge (V), and mass of active materials (g), respectively.

3. Result and discussion

The XRD patterns of as-prepared CNTs (a), CNO (b), GNO (c), and GCN (d) are illustrated in Fig. 1. Two obvious peaks with 2 θ values of 25.74° and 42.89° in as-prepared CNTs sample are the characteristic peaks of the (002) and (100) planes,^{35, 36} respectively. The diffraction peak of CNTs at 25.74° is also observed in CNO and GCN samples. The diffraction peaks of NiO are found in CNO, GNO, and GCN samples at 37.24°, 43.28°, and 62.88°, which are in well agreement with the standard diffraction card of face-centered-cubic NiO (JCPDS card no. 47-1049). However, NiO peaks in GNO are imperfect, corresponding to poor crystallinity. For the GO sample, a diffraction peak at 12.16° is consistent with (001) reflection, and after reduction, the characteristic peak of carbon from RGO could be found around 24.5°. In GNO sample, two peaks observed at 12.26° and 24.51° are associated with GO and RGO, respectively. But, no peak of GO is displayed in

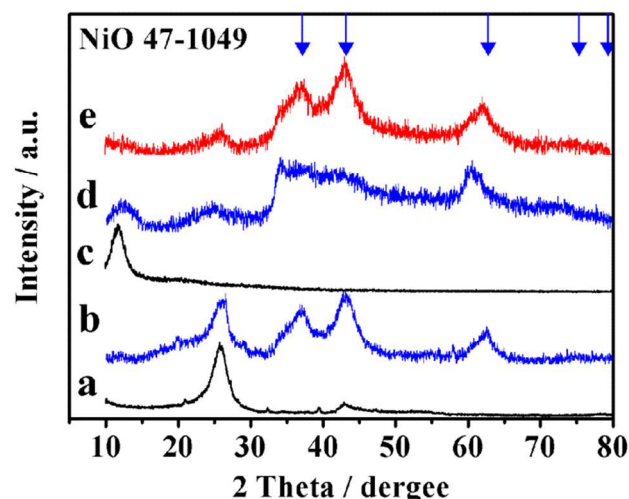


Fig. 1 XRD patterns of as-prepared CNTs (a), CNO (b), GO (c), GNO (d), and GCN (e).

GCN sample. Further examination with XPS illustrates the reduction degree of RGO. In the high-resolution C1s XPS spectra of GO, GNO, and GCN (Fig. S1), the absorbance band intensities of C-O and C(O)O in GO are much weaker in comparison with their counterparts in GNO and GCN. The ratios of C-O and C(O)O in GCN are much lower than those of GNO, indicating high reduction degree of GO in GCN.

Raman spectra are used to analyze the physical structure of carbon in these samples (Fig. 2). The G band ($\sim 1590\text{ cm}^{-1}$) is attributed to the vibration of sp^2 -bonded carbon atoms, while D band ($\sim 1350\text{ cm}^{-1}$) arises from the disorders or defects and 2D band at $\sim 2700\text{ cm}^{-1}$ is originated from a double-resonance process.⁴⁰⁻⁴³ Distinctive D and G bands around 1350 cm^{-1} and 1590 cm^{-1} are observed in all samples. The 2D bands are only found in the samples with CNTs, indicating the intact tube structure of CNTs.⁴⁴ Intensity ratio of D/G band (I_D/I_G) will increase when the structure defect increases.^{25, 45} I_D/I_G ratio is 0.56 in CNTs, exhibiting fewer structure defects. After compositing with NiO, more defects are induced during the synthesis process. Thus the I_D/I_G ratio increased to 0.72 in CNO. I_D/I_G ratios are 0.99, 1.10, and 0.87 in GO, GNO, and GCN, respectively. When GO is reduced to RGO, oxygen-containing functional groups are removed. Though the conjugated graphene network is reestablished, the size of the reestablished graphene network is usually smaller than the original graphene layer, resulting in the increase of I_D/I_G ratio.⁴⁶ Therefore, the increase of I_D/I_G ratio from 0.99 to 1.10 is reasonable. However, I_D/I_G ratio in GCN is lower than that in GNO, showing fewer structure defects. It is probably because the reduction of RGO in GCN is better than that of GNO and partial GO is substituted with CNTs, which would decrease the concentration of defects in GCN.

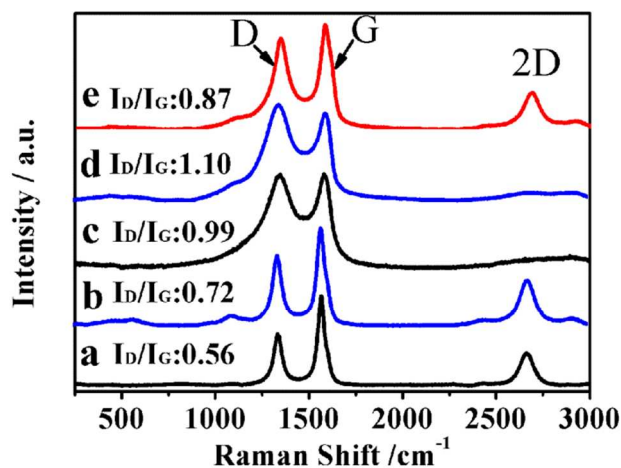


Fig. 2 Raman spectroscopy of as-prepared CNTs (a), CNO (b), GO (c), GNO (d), and GCN (e).

SEM was carried out to characterize the structures of different samples. Fig. 3 shows SEM images of CNO (a, b), GNO (c, d), and GCN (e, f) composites. CNTs and flake-like NiO are mixed together, as seen from Fig. 3a. NiO sheets with size of 100~200 nm are twined by CNTs irregularly (Fig. 3b). As exhibited in Fig. 3c, NiO and RGO are heavily aggregated in GNO, which will lead to decreased specific area. RGO sheets still have flake-like structure (Fig. 3d). In Fig. 3e and 3f, both RGO sheets and CNTs could be observed. A majority of small NiO slices are anchored on the surfaces of RGO sheets, which are separated by CNTs with less aggregation. In comparison with CNO and GNO, GCN composite is less aggregated with

more active sites exposed. CNTs insert into the interlayer of RGO as a skeleton structure to support RGO sheets and prevent them from aggregation. Meanwhile, CNTs provide the tunnels for electron transport. Thus, a good electrical conductivity is expected.

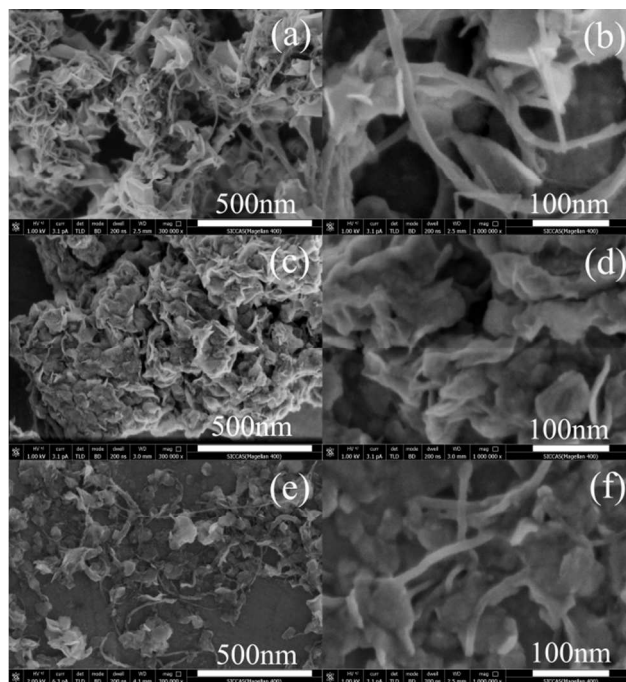


Fig. 3 SEM images of the CNO (a, b), GNO (c, d), and GCN (e, f)

To further analyze the microstructure of CNO (a, d), GNO (b, e), and GCN (c, f) composites, TEM images were taken. As shown in Fig. 4a, paper-like NiO sheets with large size are dispersed on the surface of CNTs in CNO samples. CNTs provide well skeleton structure to support NiO, which prevented the severe aggregation of NiO nanoflakes. By contrast, RGO anchored with NiO particles aggregated into bulks in GNO samples (Fig. 4b). The aggregation is caused by the intensive π - π interaction between RGO sheets. In GCN samples (Fig. 4c), NiO particles are anchored onto RGO sheets, they are connected by CNTs and form continuous network. CNTs help to avoid the aggregation among sheets. More active sites are available and electron transport properties will be improved in GCN. Crystallinities of these samples are illustrated in HRTEM images. Lattice fringes of NiO in CNO are clear and long (Fig. 4d), testifying the good crystallinity and large size of NiO. Oppositely, lattice fringes of NiO could be hardly observed in GNO samples (Fig. 4e). Only some short and dim fringes can be found, corresponding to the poor crystallinity of NiO as described in XRD analysis. In Fig. 4f, clear and short fringes indicate high crystallinity and decreased particle size of NiO in GCN. The selected area electron diffraction (SAED) results show NiO in all the composites are polycrystalline with the cubic structure.

On the basis of the above results, the synthetic processes of CNO, GNO and GCN composites are proposed as follows (Fig. 5). For CNO, negative-charged CNTs⁴⁷ attract Ni^{2+} ions by electrostatic force. Then, Ni^{2+} ions combined with OH^- provided by the hydrolyzation of urea to form $\text{Ni}(\text{OH})_2$. With the time increasing at high temperature, particle size of $\text{Ni}(\text{OH})_2$ grows larger. It is probably due to the poor solubility and tendency towards aggregation of CNTs, which could not

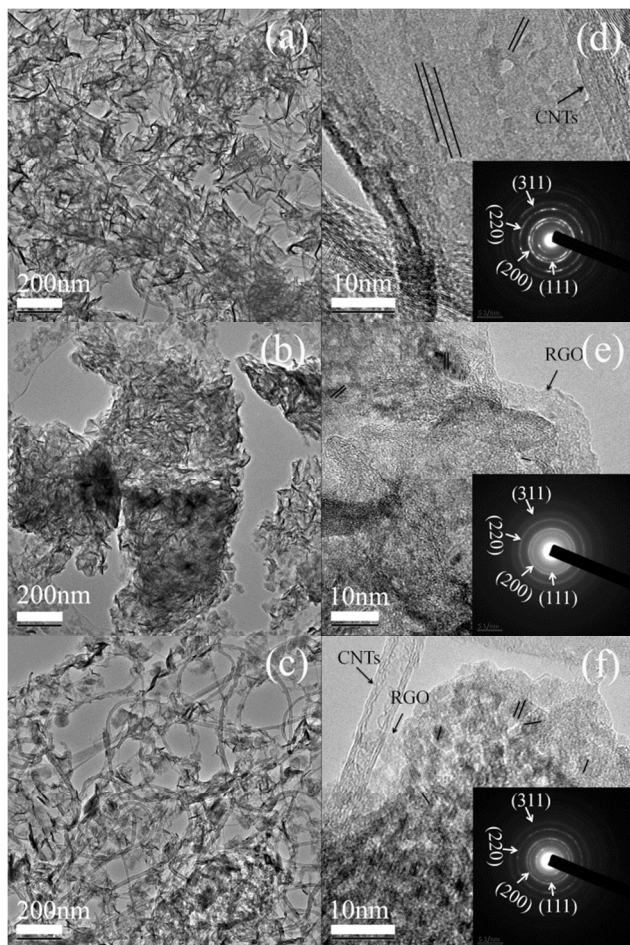


Fig. 4 TEM images of the CNO (a, d), GNO (b, e), and GCN (c, f).

restrict the growth of $\text{Ni}(\text{OH})_2$ particles. For GNO, similar process occurred, Ni^{2+} ions were attracted onto the negatively charged GO surfaces⁴⁸ and formed $\text{Ni}(\text{OH})_2$ nanoparticles. The growth of $\text{Ni}(\text{OH})_2$ particles is limited by the restricting effect of RGO, so the particle size of $\text{Ni}(\text{OH})_2$ decreased in comparison with those in CNO. GNO restacked after reduction due to the intensive π - π interaction. For GCN, CNTs and GO, both negatively charged, are dispersed homogeneously in the solution. Ni^{2+} ions will be attracted and anchored on GO preferentially due to its large specific surface areas. $\text{Ni}(\text{OH})_2$ formed with small size in GCN due to the restricting effect of RGO and transformed into NiO during the heat treatment process.

The electrochemical properties of the materials were characterized by CV and galvanostatic charge and discharge measurements. Fig. 6a presents the CV curves of CNO, GNO, and GCN samples at 5 mV s^{-1} . Each CV curve shows one redox couple. The anodic peaks are at around 0.3 V while the cathodic peaks are at around 0.5 V. The redox couples are corresponding to the faradic reaction of NiO which can be expressed by the following formula:^{19, 28}



GNO exhibits the smallest area surrounded by CV curve, indicating the smallest specific capacitance. This results from the decreasing active sites caused by aggregation of RGO/NiO. The capacitance of CNO is enhanced a little compared with

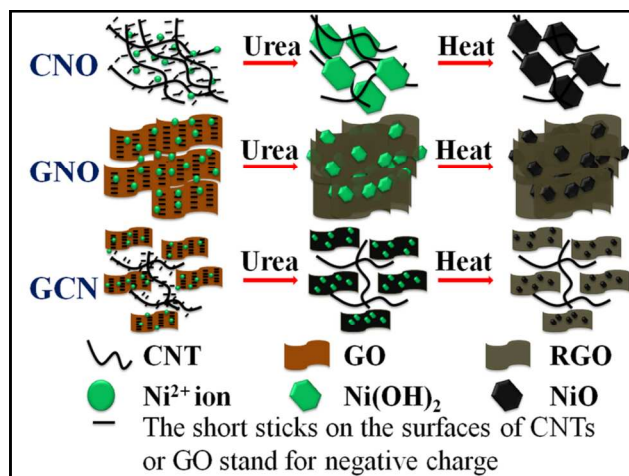


Fig. 5 Schematic illustrations of synthesis process of CNO, GNO, and GCN.

GNO. Nevertheless, NiO particles in CNO are large, which would also decrease effective area for redox reaction. Therefore, the capacitance of CNO is not high, either. The CV curve of GCN is drastically expanded, implying an enhanced capacitance. Its improved capacitive properties are attributed to uniform structure and high electrical conductivity. Fig. 6b displays the galvanostatic discharge curves of CNO, GNO, and GCN electrodes at the current density of 1 A g^{-1} . Consistent with the CV results, all samples show a typical pseudocapacitive behavior with highly nonlinear discharge curves. It is believed that the discharge time is controlled by the rate of alkali ions diffusing into and out of the surface of the electrode.²⁷ GCN electrode exhibits much longer discharge time than the other two electrodes. The prolonged discharge time is attributed to increased redox reactions caused by uniform structure and more active sites which correspond to the structural and morphological characterization as shown above.

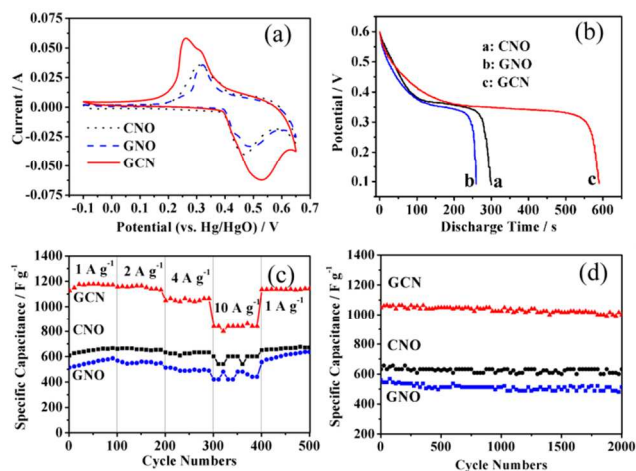


Fig. 6 (a) CV curves of CNO, GNO, and GCN electrodes at a scan rate of 555 mV s^{-1} . (b) The galvanostatic discharge curves of CNO, GNO, and GCN electrodes at 1 A g^{-1} . (c) Rate capacitance of CNO, GNO, and GCN electrodes with increasing current densities. (d) Cyclic performance of CNO, GNO, and GCN electrodes at 4 A g^{-1} .

To further analyze the electrochemical performance of CNO, GNO, and GCN electrodes, they were tested at different current

densities. Fig. 6c displays rate capacitance of CNO, GNO, and GCN electrodes with increasing current density. Under the same conditions, the specific capacitance of the GCN electrode is much higher than those of CNO and GNO electrodes. GCN electrode takes the dual advantages of CNTs and RGO, leading to the great enhancement in capacitance. Is not only the conductivity improved by CNTs but also more active sites are contributed by smaller NiO on RGO. Through calculation, the specific capacitances at 1 A g^{-1} are 660, 580 and 1180 F g^{-1} for CNO, GNO, and GCN, respectively. Capacitance will decrease with the current density increasing. For GCN electrode, the specific capacitance drops to 1050 F g^{-1} at 4 A g^{-1} , while the specific capacitances of CNO and GNO are only 630 and 490 F g^{-1} under the similar condition, respectively. Even at high current density of 10 A g^{-1} , the specific capacitance of GCN is still as high as 840 F g^{-1} , which is much higher than those of CNO (600 F g^{-1}) and GNO (420 F g^{-1}). Fig. 6d displays the cyclability of CNO, GNO, and GCN electrodes at 4 A g^{-1} . The capacity retention ratios of CNO, GNO, and GCN are 95 %, 87 %, and 95 %, respectively. The capacitance of GCN is still as high as 1000 F g^{-1} even after 2000 cycles, certifying excellent cycling stability.

Electrochemical impedance spectroscopy illustrates the electron transport properties of these samples. Fig. 7 shows the Nyquist plots of CNO (a), GNO (b) and GCN (c) electrodes. Each spectrum displays a depressed semicircle in high-frequency region and a straight line in low-frequency region. It is well accepted that the semicircle corresponds to the charge transfer resistance, which is related to the surface area and electrical conductivity.^{49, 50} GCN electrode exhibits smallest semicircle, indicating that GCN electrode has lower charge transfer resistance than the other two electrodes. Because tunnels for electron transport provided by CNTs and more available active sites decrease the charge transfer resistance. The straight line reflects the diffusion of the electro-active species.⁵¹ The nearly vertical line indicates rapid ion diffusion in the electrolyte and adsorption onto the electrode surface.⁵² CNO and GCN show nearly vertical shapes because electrons could transfer fast due to less aggregation and tunnels provided

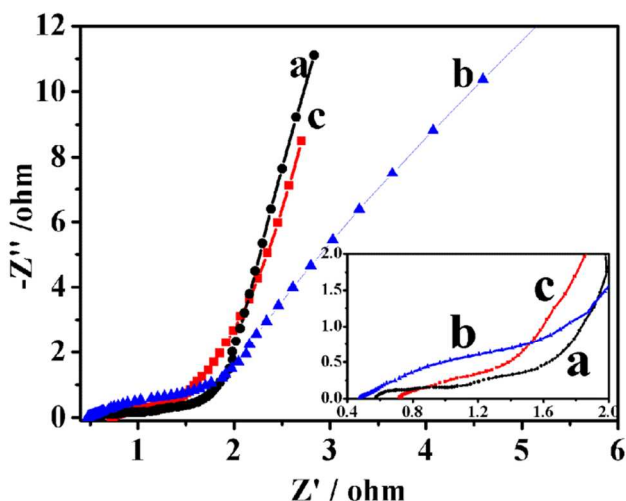


Fig. 7 Electrochemical impedance spectra (EIS) obtained from CNO (a), GNO (b) and GCN (c) electrodes. The inset shows the enlarged EIS of the electrodes.

by CNTs. GNO exhibits the smallest slope of straight line, which corresponds to the limitation of ion diffusion caused by aggregated RGO/NiO sheets.

Based on the above electrochemical analysis, GCN showed excellent capacitive and cycling performance even at considerably high charge and discharge currents. The reason for this can be well understood if the following factors are considered. First, the aggregation of RGO coated with NiO is obviously lessened by the addition of CNTs, which could increase effective area of GCN composite for redox reaction. Particle size of NiO is significantly reduced and more active sites are available in redox reaction. Second, CNTs provide more tunnels for electron and ion transport to enhance the electric conductivity of GCN electrode. Third, RGO and CNTs act as structural buffer for the large volume expansion of NiO during the redox process. The unique architecture, high crystallinity, high conductivity and excellent dispersion state synergistically enhance the capacity and cycling performance of the GCN electrode.

4. Conclusions

We demonstrated an effective strategy for preventing the RGO/NiO from aggregation via a simple method under facile conditions. The addition of GNTs is the key factor that separates the RGO/NiO sheets. A high specific capacitance of 1180 F g^{-1} can be achieved for RGO/CNTs/NiO composite. The excellent electrochemical performance is a result of the synergistic effect. NiO particles with high crystallinity and decreased particle size distribute homogeneously on the RGO surface. The enhanced reduction degree of GO and tunnels for electron transport provided by CNTs improve the electron transport properties. Thus, GCN shows higher specific capacitance, better cyclicality and stability than those of CNO and GNO, which is promising for large-capacity energy storage.

Acknowledgements

This work is supported by the National Basic Research Program of China (2012CB932303) and the National Natural Science Foundation of China (Grant No. 51072215 and 51172261).

Notes and references

- ⁹⁰ The State Key Lab of High Performance Ceramics and Superfine Microstructure, Shanghai Institute of Ceramics, Chinese Academy of Sciences, 1295 Dingxi Road, Shanghai 200050, P.R. China
Email address: jingsun@mail.sic.ac.cn; liagao@mail.sic.ac.cn.
Tel.: +86-21-52414301; Fax: +86-21-52413122.
- ⁹⁵ Electronic Supplementary Information (ESI) available: Fig. S1, Table S1. See DOI: 10.1039/b000000x/
1. C. Y. Chen, C. Y. Fan, M. T. Lee and J. K. Chang, *Journal of Materials Chemistry*, 2012, **22**, 7697-7700.
2. H. S. C. Hailiang Wang, Yongye Liang and Hongjie Dai, *J.A.M. CHEM. SOC.*, 2010, **132**, 7472-7477.
3. C. Liu, F. Li, L.-P. Ma and H.-M. Cheng, *Advanced Materials*, 2010, **22**, E28-E62.
4. P. J. Sumanta Kumar Meher, and G. Ranga Rao, *ACS Applied Materials & Interfaces*, 2011, **3**, 2063-2073.

5. J. Z. Sheng Chen, Xiaodong Wu, Qiaofeng Han, and Xin Wang, *ACS Nano*, 2010, **4**, 2822-2830.
6. J. Liu, J. Jiang, C. Cheng, H. Li, J. Zhang, H. Gong and H. J. Fan, *Advanced Materials*, 2011, **23**, 2076-2081.
7. S. P. Meryl D. Stoller, Yanwu Zhu, Jinho An, and Rodney S. Ruoff, *Nano Letters*, 2008, **8**, 3498-3502.
8. B. E. Conway, *Plenum Publishers*, New York 1999.
9. X. Sun, G. Wang, J. Hwang and J. Lian, *Journal of Materials Chemistry*, 2011, **21**, 16581-16588.
10. Y. P. Zhai, Y. Q. Dou, D. Y. Zhao, P. F. Fulvio, R. T. Mayes and S. Dai, *Advanced Materials*, 2011, **23**, 4828-4850.
11. N. Zhang, J. Sun, D. Jiang, T. Feng and Q. Li, *Carbon*, 2009, **47**, 1214-1219.
12. W. R. Zhong-Shuai Wu, Da-Wei Wang, Feng Li, Bilu Liu, and Hui-Ming Cheng, *ACS Nano*, 2010, **4**, 5835-5842.
13. M. Noked, A. Soffer and D. Aurbach, *Journal of Solid State Electrochemistry*, 2011, **15**, 1563-1578.
14. J. Li, W. Zhao, F. Huang, A. Manivannan and N. Wu, *Nanoscale*, 2011, **3**, 5103-5109.
15. Y. L. Lu Liu, Shuming Yuan, Ming Ge, Manman Ren, Chunsheng Sun, and Zhen Zhou, *J. Phys. Chem. C*, 2010, **114**, 251-255.
16. C. Xu, X. Wang, J. Zhu, X. Yang and L. Lu, *Journal of Materials Chemistry*, 2008, **18**, 5625-5629.
17. X.-L. Huang, J. Chai, T. Jiang, Y.-J. Wei, G. Chen, W.-Q. Liu, D. Han, L. Niu, L. Wang and X.-B. Zhang, *Journal of Materials Chemistry*, 2012, **22**, 3404-3410.
18. R. B. Rakhi, W. Chen and H. N. Alshareef, *Journal of Materials Chemistry*, 2012, **22**, 5177-5183.
19. X. Zhang, W. Shi, J. Zhu, W. Zhao, J. Ma, S. Mhaisalkar, T. L. Maria, Y. Yang, H. Zhang, H. H. Hng and Q. Yan, *Nano Research*, 2010, **3**, 643-652.
20. C.-Y. Cao, W. Guo, Z.-M. Cui, W.-G. Song and W. Cai, *Journal of Materials Chemistry*, 2011, **21**, 3204-3209.
21. H. Yang, G. H. Guai, C. Guo, Q. Song, S. P. Jiang, Y. Wang, W. Zhang and C. M. Li, *The Journal of Physical Chemistry C*, 2011, **115**, 12209-12215.
22. X. Xia, J. Tu, Y. Mai, R. Chen, X. Wang, C. Gu and X. Zhao, *Chemistry European Journal*, 2011, **17**, 10898-10905.
23. P. Lin, Q. J. She, B. L. Hong, X. A. J. Liu, Y. N. Shi, Z. Shi, M. S. Zheng and Q. F. Dong, *J Electrochem Soc*, 2010, **157**, A818-A823.
24. H. Y. Koo, H.-J. Lee, H.-A. Go, Y. B. Lee, T. S. Bae, J. K. Kim and W. S. Choi, *Chemistry - A European Journal*, 2011, **17**, 1214-1219.
25. D. Luo, G. Zhang, J. Liu and X. Sun, *The Journal of Physical Chemistry C*, 2011, **115**, 11327-11335.
26. D. Chen, X. Wang, T. Liu, X. Wang and J. Li, *ACS Applied Materials & Interfaces*, 2010, **2**, 2005-2011.
27. X. Zhu, H. Dai, J. Hu, L. Ding and L. Jiang, *Journal of Power Sources*, 2012, **203**, 243-249.
28. B. Zhao, J. Song, P. Liu, W. Xu, T. Fang, Z. Jiao, H. Zhang and Y. Jiang, *Journal of Materials Chemistry*, 2011, **21**, 18792-18798.
29. B. You, L. Wang, L. Yao and J. Yang, *Chemical communications*, 2013, **49**, 5016-5018.
30. H. Pan, J. Li and Y. Feng, *Nanoscale research letters*, 2010, **5**, 654-668.
31. Y. Zhai, Y. Dou, D. Zhao, P. F. Fulvio, R. T. Mayes and S. Dai, *Advanced Materials*, 2011, **23**, 4828-4850.
32. Z. Fan, J. Chen, K. Cui, F. Sun, Y. Xu and Y. Kuang, *Electrochimica Acta*, 2007, **52**, 2959-2965.
33. W. S. H. Jr and R. E. Offeman, *J. Am. Chem. Soc.*, 1958, **80** 1339-1339.
34. H. Xia, Y. S. Meng, G. Yuan, C. Cui and L. Lu, *Electrochemical and Solid-State Letters*, 2012, **15**, A60-A63.
35. J.-B. Park, G.-S. Choi, Y.-S. Cho, S.-Y. Hong, D. Kima, S.-Y. Choi, J.-H. Lee and K.-I. Cho, *J Cryst Growth*, 2002, **244** 211-217.
36. T. H. Yoon and Y. J. Park, *Nanoscale research letters*, 2012, **7**, 28-31.
37. B. Li, H. Cao, J. Yin, Y. A. Wu and J. H. Warner, *Journal of Materials Chemistry*, 2012, **22**, 1876.
38. Z. Gao, J. Wang, Z. Li, W. Yang, B. Wang, M. Hou, Y. He, Q. Liu, T. Mann, P. Yang, M. Zhang and L. Liu, *Chemistry of Materials*, 2011, **23**, 3509-3516.
39. Y. Xu, K. Sheng, C. Li and G. Shi, *ACS Nano*, 2010, **4** (7), 4324-4330.
40. F. Yang, Y. Liu, L. Gao and J. Sun, *J. Phys. Chem. C*, 2010, **114**, 22085-22091.
41. C.-Y. Su, Y. Xu, W. Zhang, J. Zhao, X. Tang, C.-H. Tsai and L.-J. Li, *Chemistry of Materials*, 2009, **21**, 5674-5680.
42. M. Li, J. E. Zhu, L. Zhang, X. Chen, H. Zhang, F. Zhang, S. Xu and D. G. Evans, *Nanoscale*, 2011, **3**, 4240-4246.
43. H. Li, G. Zhu, Z.-H. Liu, Z. Yang and Z. Wang, *Carbon*, 2010, **48**, 4391-4396.
44. Z. Wen, X. Wang, S. Mao, Z. Bo, H. Kim, S. Cui, G. Lu, X. Feng and J. Chen, *Adv Mater*, 2012, **24**, 5610-5616.
45. Z. Tai, X. Yan and Q. Xue, *Journal of Power Sources*, 2012, **213**, 350-357.
46. Z. Ji, X. Shen, G. Zhu, H. Zhou and A. Yuan, *Journal of Materials Chemistry*, 2012, **22**, 3471-3478.
47. H. Hu, A. Yu, E. Kim, B. Zhao, M. E. Itkis, E. Bekyarova and R. C. Haddon, *The journal of physical chemistry. B*, 2005, **109**, 11520-11524.
48. J. T. Chen, Y. J. Fu, Q. F. An, S. C. Lo, S. H. Huang, W. S. Hung, C. C. Hu, K. R. Lee and J. Y. Lai, *Nanoscale*, 2013, **5**, 9081-9088.
49. S.-E. Chun, S.-I. Pyun and G.-J. Lee, *Electrochimica Acta*, 2006, **51**, 6479-6486.
50. Y.-Y. Horng, Y.-C. Lu, Y.-K. Hsu, C.-C. Chen, L.-C. Chen and K.-H. Chen, *Journal of Power Sources*, 2010, **195**, 4418-4422.
51. L. Wang, Z. H. Dong, Z. G. Wang, F. X. Zhang and J. Jin, *Advanced Functional Materials*, 2013, **23**, 2758-2764.
52. M. Kim, Y. Hwang and J. Kim, *Journal of Power Sources*, 2013, **239**, 225-233.